Investigation of multilayered aluminium-coated polymer laminates by focused ion beam (FIB) etching

S. Brunner [a], Ph. Gasser [b], H. Simmler [a], K. Ghazi Wakili [a,*]

[a] *Laboratory for Applied Physics in Building, Swiss Federal Laboratories for Materials Testing and Research (Empa), CH-8600 Duebendorf, Switzerland*
[b] *Laboratory for Concrete/Construction Chemistry, Swiss Federal Laboratories for Materials Testing and Research (Empa), CH-8600 Duebendorf, Switzerland*

Abstract

Multilayered aluminium-coated polymer laminates are the common barrier envelopes of vacuum insulation panels used as thermal insulations in building applications. These laminates are made of up to ten distinct layers including three barrier layers made by vacuum web coating. The thickness of each aluminium layer (30–100 nm) influences the overall thermal performance of the panels as well as the temperature at joints between adjacent panels. Two commercially available barrier envelopes have been investigated by means of focused ion beam etching for an adequate determination of the effective thickness of the aluminium layers. Additional information has been gained on interfacial failure between aluminium and its neighbouring polymeric film or adhesive layer as well as disruptions in the aluminium layer itself. These provide hints related to air and moisture permeation, the key properties of barrier envelopes in building applications where a lifetime of 20 to 50 years is required.
© 2005 Elsevier B.V. All rights reserved.

1. Introduction

The continuous tightening of energy consumption regulations fostered research activities in the domain of high performance insulation materials. Vacuum insulation panels (VIP) consisting of an evacuated core and an air and moisture tight barrier envelope were developed first for use in the refrigeration industry and later extended to applications in insulating the building [1]. One such panel is shown in Fig. 1 with a cross-section through its corner. The barrier envelope of the VIP has to fulfil several requirements. First, it has to maintain a low pressure not exceeding an acceptable level in the core during a period of 20–30 years. For nano-structured core materials, this pressure level is around 100 mbar [1,2] at the end of the service life. Second, the thermal short circuit at the VIP edges induced by lateral heat flow has to be kept at a minimum [3]. Third, the material has to have enough elasticity and tear resistance to enable packaging, welding on the boundaries and general handling. It seems that for the time being a multilayered

aluminium-coated polymer laminate meets the above requirements best. Investigations were carried out on two such laminates (L1 and L2) used for commercially available VIPs. A schematic representation is given in Fig. 2 (not scaled for reason of visibility). The aluminium layers fulfil the role of tight and durable air and moisture barriers but dominate the thermal bridge effect at the joints of adjacent VIPs. The reason for this dominance lies in the high thermal conductivity of aluminium ($\lambda_{Al, pure} = 210$ W m^{-1} K^{-1}) compared to the conductivity of the core (0.004 W m^{-1} K^{-1} in dry condition) and the polymer layers (0.25–0.30 W m^{-1} K^{-1}). This, in spite of the very low thickness of the aluminium layers, summed up to 90–300 nm. Hence the thickness of these metallic layers is of great importance and has to be determined with sufficient precision. Conventional methods such as mechanical cutting/polishing and cryo-breaking (at low temperatures) are not appropriate when dealing with thicknesses of 30 nm to 100 nm and these types of polymeric multilayered laminates. The focused ion beam etching (FIB) is a well established method for the study of microstructures and interfaces [4–6] and has been used as a valuable tool in different technologies [7,8]. The present paper reports on the thickness analysis of the aluminium layers of the

---

* Corresponding author. Fax: + 41 1 823 40 09.
  E-mail address: karim.ghaziwakili@empa.ch (K.G. Wakili).
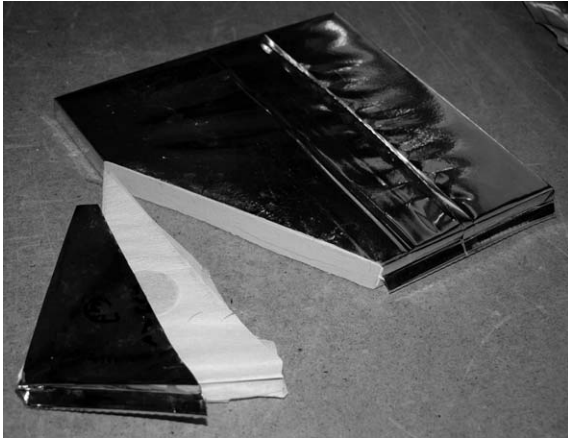
Fig. 1. Cross section through a corner of a vacuum insulated panel VIP ($250 \times 250 \times 20$ mm^3) with fumed silica as core material and a multilayered aluminium-coated polymer laminate as barrier envelope.

mentioned two laminates (L1 and L2) by means of the focused ion beam FIB etching method and the results thereof.

2. Production of the barrier envelopes

Both investigated laminates are commercially available products of two industrial producers of high barrier envelopes. According to the information received the two laminates have undergone different production sequences. This is of major importance for the discussion of the results. For Laminate L1 a metallized PET film produced by aluminium vacuum web coating was used. The production started with laminating the first metallized PET (layers D+C in Fig. 2a) to the LDPE film (layer A in Fig. 2a) by means of a gluing PU layer (layer B in Fig. 2a). Then two similar steps followed laminating the second and the third metallized PET film. With respect to mechanical stress, it has to be added that the laminate was wound and unwound several times during its production process. The PET film was rewound right after being metallized. Then in each lamination process it was

unwound at the beginning and rewound at the end. For laminate L2, a metallized PET film and a metallized PP film were used. Both film types were metallized by aluminium vacuum web coating. The production started with laminating the first metallized PET film (layers J+I in Fig. 2b) to the metallized PP film (layers F+G in Fig. 2b) by means of a gluing PU layer (H in Fig. 2b). Then a second metallized PET film (layers C+D in Fig. 2b) was added using again a gluing PU layer (E in Fig. 2b). As a final step, a LDPE film (layer A in Fig. 2b) was added to the laminate similarly.

3. Sample preparation and experimental setup

Samples of about 1×1 cm^2 were cut out of both types of VIP barrier envelopes. These were subject to mechanical stress visible in form of wrinkles arising from the vacuum packaging. Each sample was fixed with carbon tape to a standard microscope stub and coated with a layer of approximately 10 nm of Au to improve conductivity. Sample cross-sections have been prepared with a FEI Strata DB 235 dual beam (DB) focused ion beam (FIB) workstation. The dual beam workstation incorporates a focused ion beam and a scanning electron microscope (SEM) column tilted to each other at an angle of 52° (Fig. 3). The operating principle of a focused ion beam machine is comparable to a SEM, but instead of electrons, a focused beam of Ga$^+$ ions is scanned across the sample surface. A focused beam of the same Ga$^+$ ions with a 100-times higher intensity is used to prepare a cross-sectional view by milling i.e. removal of material. The SEM column is equipped with a field emission electron source, an in-lens detector, a secondary electron detector and a secondary ion detector. The resolution of the E-beam imaging is specified to be 3 nm at 5 kV. The FIB column is adjustable from 1 pA to 20,000 pA at 30 kV with a specified resolution of 7 nm. The workstation has a digital patterning generator and four gas injection systems. Two of these injection systems have been used for the present investigation, one for platinum deposition with $(CH_3)3$ Pt $(CpCH_3)$ where Cp stands for cyclopentadienyl and one for a selective carbon mill process

J	PET	Polyethylene terephtalate	12 µm
I	AL	Aluminium	100 nm = 0.1 µm
H	PU	Polyurethane	2 µm
G	PET	Polyethylene terephtalate	12 µm
F	AL	Aluminium	100 nm = 0.1 µm
E	PU	Polyurethane	2 µm
D	PET	Polyethylene terephtalate	12 µm
C	AL	Aluminium	100 nm = 0.1 µm
B	PU	Polyurethane	2 µm
A	LDPE	Low Density Polyethylene	50 µm

a) Laminate L1

J	PET	Polyethylene terephtalate	12 µm
I	AL	Aluminium	30 nm = 0.03 µm
H	PU	Polyurethane	2 µm
G	AL	Aluminium	30 nm = 0.03 µm
F	PP	Polypropylene	18 µm
E	PU	Polyurethane	2 µm
D	AL	Aluminium	30 nm = 0.03 µm
C	PET	Polyethylene terephtalate	12 µm
B	PU	Polyurethane	2 µm
A	LDPE	Low Density Polyethylene	60 µm

b) Laminate L2

Fig. 2. Structure of the two investigated barrier envelopes according to the manufacturers with a total thickness of a) 92 µm and b) 108 µm (not scaled).
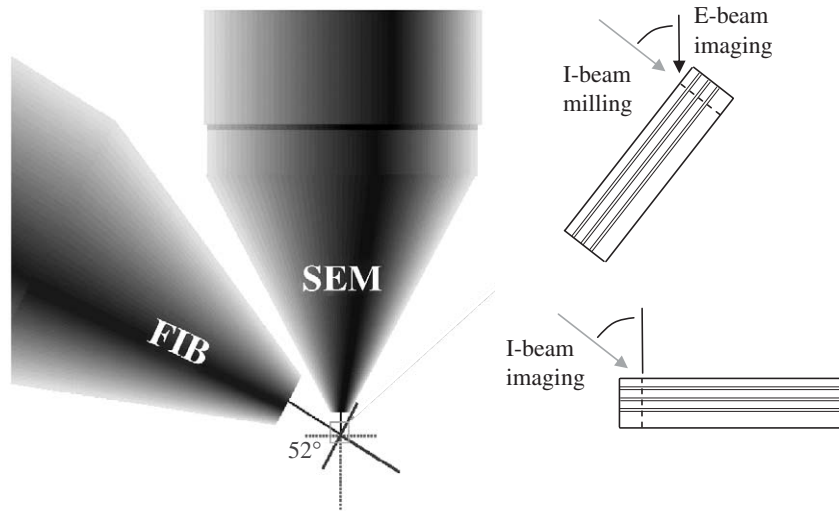
Fig. 3. Schematic representation of the FIB assembly (left). The cross-sectional surface (dotted line) is at an angle of 52° (machine coordinates) during I-beam milling and E-beam imaging (upper right) and at an angle of 0° during I-beam imaging (lower right).

($MgSO_4 \cdot 7H_2O$). The platinum layer was used when the uppermost polymer layer had to be protected in order to determine its thickness. The cross-section was milled in several steps. In a first step a regular cross-section pattern was milled with 20,000 pA together with the mentioned carbon mill process. As the samples were relatively thick (100 μm) compared to common FIB operating standards (5–10 μm), an operating time of up to 3 h was needed to perform the etching of a regular cross-section (50×20 μm^2). For polishing the cross-section, a beam current of 3000 pA or 1000 pA was used subsequently. The milling time depends on the required quality of the surface. Fig. 4 left shows the sample edge seen by the I-beam in its milling orientation. Fig. 4 right represents the position of the layers with respect to the cross-sectional cut and the different beam directions. Investigation of the cross-section was performed either by I-beam or by E-beam. In case of I-beam investigations, a low current (about 10 pA) was used. E-beam images were taken with 5 kV.

4. Results and discussions

Figs. 5a and b show the visualization of laminate L1 by means of the two imaging techniques. The I-beam technique is obviously able to distinguish between the different polymer layers whereas the E-beam contrasts better the metallic layers from nonmetallic ones. Fig. 6a showing a magnified part of Fig. 5b enables the distinction of each single layer according to Fig. 2a. An irregularity between the aluminium layer C and its neighbouring layers B (PU) and D (PET) is clearly visible. This is a rupture either between the layer C (AL) and its adjacent adhesive layer B (PU) or between the layer C (AL) and its substrate layer D (PET). A nearer zoom of this detail with a magnification of 80,000 (Fig. 6b) shows a cavern surface with similarity to metallic grain boundaries on top of layer B. This makes the second rupture type likely. The upper bright line in Fig. 6b is due to charge accumulation caused by the I-beam on the geometric edge of the cavern, not to be confused with the
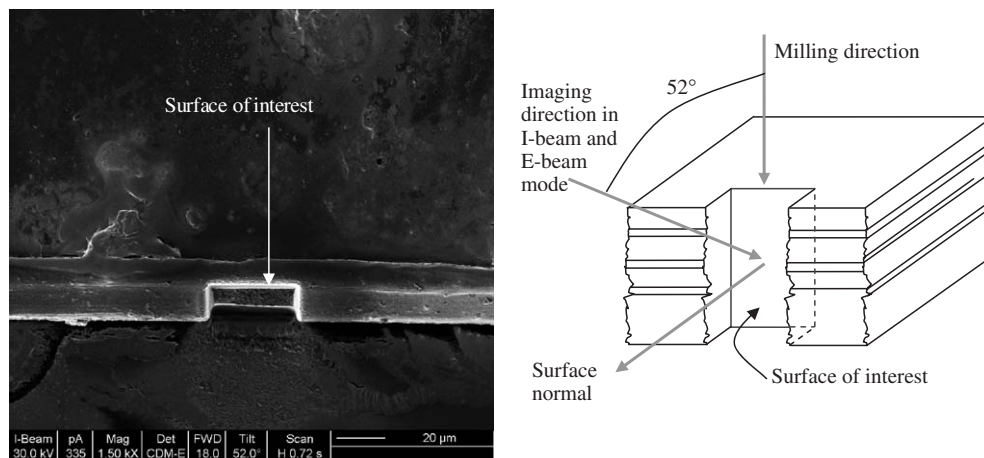
Fig. 4. Edge of the sample seen by the I-beam with milling direction at a tilt angle of 52°. The surface of interest (right) shrinks to a bright line (left) when looking in the milling direction.
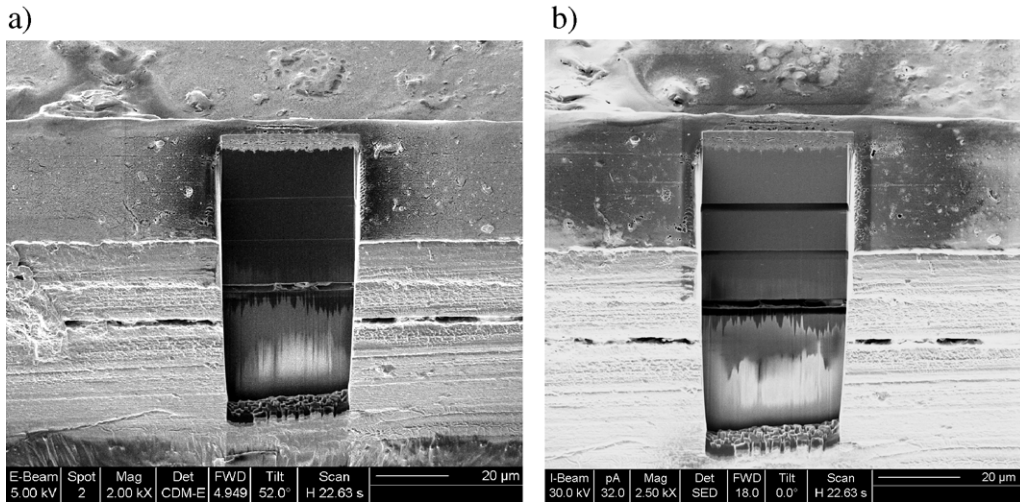
Fig. 5. The E-beam a) and the I-beam b) imaging of laminate L1. The vertical scale is shortened by sine (52°) as in all following figures.
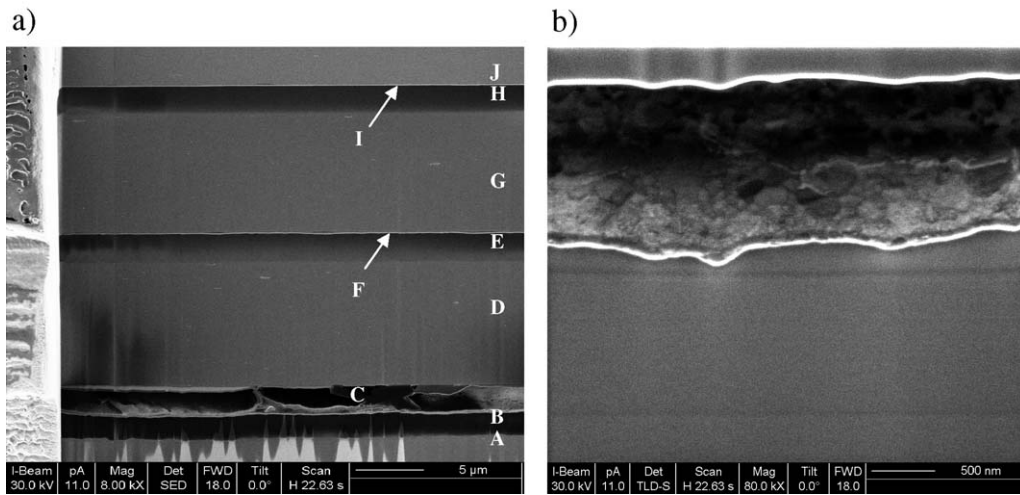
Fig. 6. Details of I-beam imaging at different scales showing a) the structure of laminate L1 with a disruption gap at layer C and b) view into the gap at layer C at another cross section.
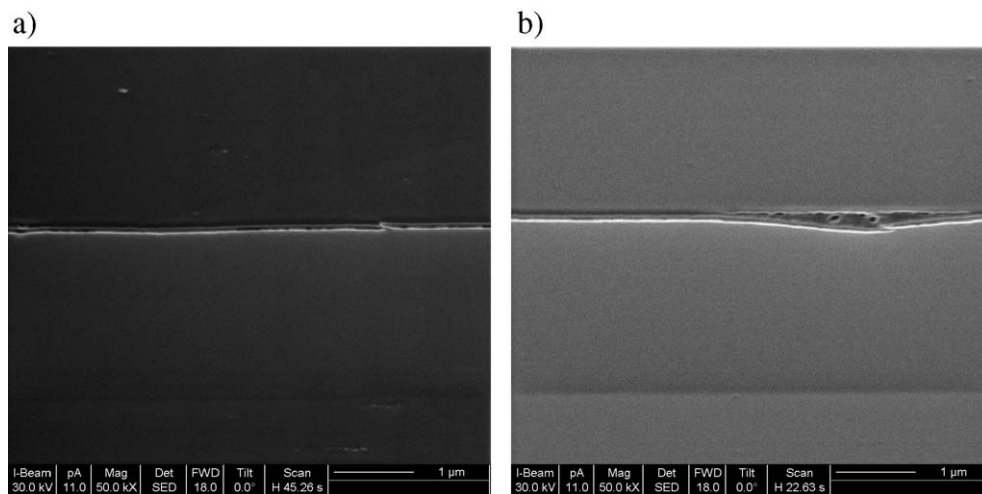
Fig. 7. Disruptions in the second aluminium layer (F) of laminate L1 at sites without a) and with b) surface impurities on its substrate (G).
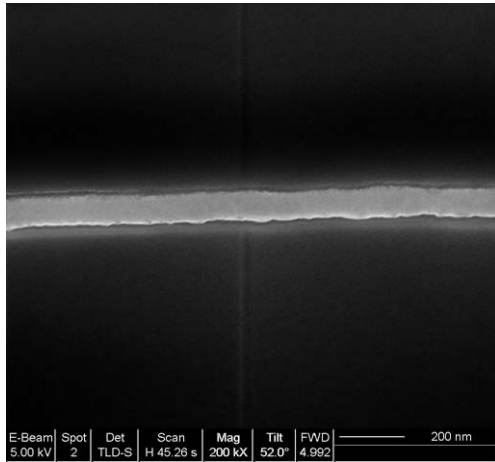
Fig. 8. E-beam imaging of laminate L1 yielding the thickness of the aluminium layer (F). A correction of Sine 52°=0.79 for the tilt angle has to be included when measuring vertical dimensions.

Fig. 10. Further magnification of laminate L2 representing a detail of Fig. 9, showing disruptions in the aluminium layer G and a part of the gas bubble in the PU layer H (bright at right).

lower bright line representing an aluminium layer. Fig. 7a shows a disruption in the second aluminium layer (F) generated by mechanical stress probably due to the production process. This kind of disruption is also found at sites where interface impurities between the aluminium layer (F) and its substrate (G) exist (Fig. 7b). It is likely that this impurity was already present prior to the metallization process despite the foregoing plasma cleaning. Going back to the E-beam imaging with a resolution of 3 nm as mentioned earlier the absolute thickness of each aluminium layer (C, F and I) can be determined with sufficient accuracy (Fig. 8) keeping in mind a correction of Sine 52° due to the tilt angle. Similarly, the layers of laminate L2 can be identified. Fig. 9a shows these layers with the nomenclature corresponding to Fig. 2b. In order to comply with the layer sequence of Fig. 2b, all the following figures were turned upside down. The metallic layers D, G and I are recognizable as bright lines. Defects in form of gas bubbles are present in the PU layer (H). Most probably this is due carbon dioxide

originating from the stoichiometric deviations in the PU components. In this case, the gas is trapped between two low permeating aluminium layers (G and I). In all other PU layers where at least one of the adjacent layers is a polymeric material, the gas is absorbed in the latter. A four times larger magnification (12,000) of such a bubble is shown in Fig. 9b. A further magnification (Fig. 10) shows disruptions in the aluminium layer G coated on the PP film. As the PET film is stiffer than the PP film the aluminium layer coated on it, (I) seems to have fewer disruptions if any. The notion of artefacts in microscopic imagery has to be kept in mind. A rigorous discussion of this for the present method applied to laminates with thin metallic layers in combination with relatively thick polymer layers is still lacking. Different authors [9–11] have reported that no apparent damages due to milling were visible on their result. Another author [12] mentions damages on polymer caused by metal deposition on the polymer only. Milling-induced artefacts on inorganic materials, especially

a)

b)
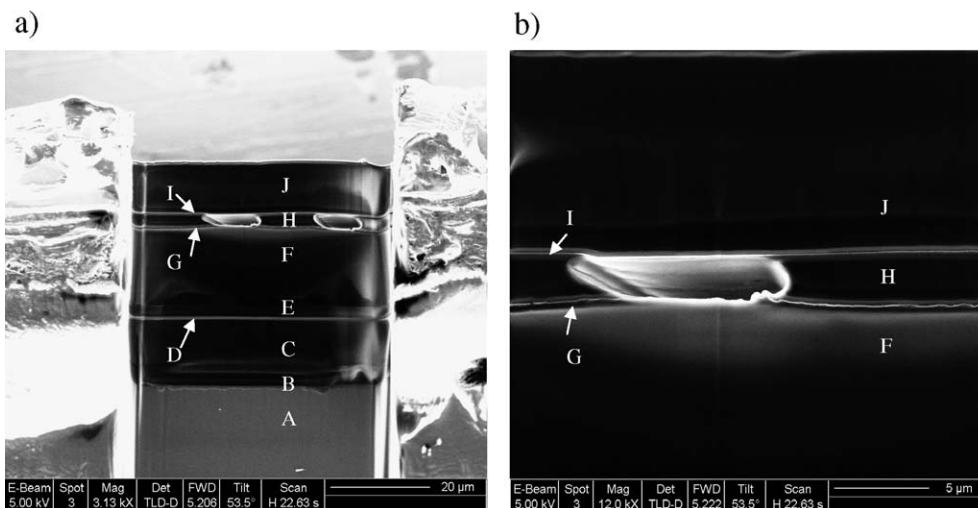
Fig. 9. Details of E-beam imaging at different scales showing a) the structure of laminate L2 and b) 4 times zoom into the gas bubbles appearing in the PU layer H (for nomenclature see Fig. 2b).

Table 1
Thickness of the different material layers according to the manufacturers compared to values determined by E-beam and I-beam imaging

Laminate	Layer	Thickness declared (μm)	Thickness measured (μm)	Magnification x1000
L1	A	50	–	–
	B	2	2.0 ± 0.3	25
	C	0.100	0.115 ± 0.010[a]	150–200
	D	12	12.5 ± 1.0	8–10
	E	2	2.5 ± 0.3	25
	F	0.100	0.115 ± 0.010[a]	150–200
	G	12	12.0 ± 1.0	8–10
	H	2	2.6 ± 0.3	25
	I	0.100	0.115 ± 0.010[a]	150–200
	J	12	12.5 ± 1.0	8–10
L2	A	60	57 ± 4	8–10
	B	2	4.6 ± 1.5	25
	C	12	11.8 ± 1.0	8–10
	D	0.030	0.052 ± 0.008[a]	150–200
	E	2	2.7 ± 0.5	25
	F	18	19 ± 1.5	8–10
	G	0.030	0.058 ± 0.009[a]	150–200
	H	2	2.9 ± 0.5	25
	I	0.030	0.052 ± 0.008[a]	150–200
	J	12	12.5 ± 1.0	8–10

The nomenclature of the layers (aluminium layers are highlighted) corresponds to Fig. 2.
[a] Using the results of E-beam imaging only.

semiconductors, are the topic of several papers [13–15]. As our focus in this paper is on the thickness of aluminium layers, the polishing after the coarse milling was not performed on all the cross-sectional surfaces. So the vertical line structure in Fig 5a,b on the lower part represent coarse milled but not polished surfaces. This structure is enlarged in Fig. 6a at lower part of the image. The single vertical line in Figs. 8 and 9b is the so-called waterfall effect occurring in the fine milled areas. The gap in Figs. 5 and 6a) might be caused by one of the many wrinkles of the envelope due to evacuation. For the cross-section in Fig. 5, it cannot be excluded that it originated from a nearby scissors cut. A similar type of gap was found in a sample from the corner part of a vacuum insulation panel, i.e. far away from the scissors cut (at least 10 mm). The use of cryo-microtomy in combination with FIB [16] might be an option to reduce caused shear forces, hence allow better investigation of gaps. In Fig. 10 the disruption of the aluminium layer G might be caused as well by sample preparation as by wrinkles. These are abundant on the foil due to the core shrinking caused by evacuation. A summary of the declared and measured layer thicknesses for both laminates is given in Table 1. The measured values of the aluminium layers, the main purpose of this study, were extracted from E-beam imaging on two different milling sites for both laminates. In order to get representative values, images with magnifications between 50,000 and 200,000 were used. The thickness of the polymer layers was determined from E-beam and I-beam images with a magnification in the range of 8000 to 25,000 for the sake of completeness. The uncertainties indicated in Table 1 result from thickness fluctuations of the layers due to production and handling and are larger than the

resolution of the imaging method itself (3 nm for E-beam and 7 nm for I-beam). The standard deviation results from at least 4 measurement sets. As the three aluminium layers of laminate L1 (C, F and I in Fig. 2a) originate from the same metallized PET film, no distinction has been made between when determining the average thickness and its deviation. The same applies to the layers D and I of laminate L2. The layer G (Fig. 2b) has been treated separately.

5. Conclusion and outlook

The FIB-etching and the subsequent E-beam imaging allow determining the thickness of aluminium layers down to 30 nm otherwise hardly measurable. The thickness of these layers is crucial for the additional heat loss through vacuum insulation panels. Their barrier envelopes contain such thin aluminium layers to minimize gas and moisture permeation into the core. Besides determining the thickness of the aluminium layers for two commercially available laminates additional information could be extracted regarding interfacial failure between aluminium and its neighbouring polymeric film or adhesive as well as disruptions in the aluminium layer itself. This may be of great importance when studying the permeation rate of air and moisture which in turn affects the aging of vacuum insulation panels, the subject of another publication [17]. The gas transport by means of thermally activated diffusion and transport through defects has been broadly discussed in a review [18] for a variety of oxide coated polymeric substrates with respect to aluminium as a reference coating. Other authors [19,20] have pointed out the importance of microscopic defects and grain boundaries on the water vapour and oxygen permeation rate through inorganic barrier layers including numerical simulation of permeation through pinholes. A systematic investigation of such defects by means of the FIB-method aiming to get more insight into the mechanisms of permeation seems to be promising.

References

[1] IEA Annex 39 "High Performance Thermal Insulation in Building and Building Systems", final report, online at www.vip-bau.ch.
[2] R. Caps, U. Heinemann, M. Ehrmanntraut, J. Fricke, High Temp., High Press. 33 (2001) 151.
[3] K. Ghazi Wakili, R. Bundi, B. Binder, Build. Res. Inf. 32 (2004) 293.
[4] F.A. Khalid, O. Beffort, U.E. Klotz, B.A. Keller, P. Gasser, S. Vaucher, Acta Mater. 51 (2003) 4575.

[5] M.W. Phaneuf, Micron 30 (1999) 277.

[6] U. Sennhauser, P. Jacob, Ph. Gasser, Pract. Metallogr. 41 (2004) 199.

[7] S. Tsuji, K. Tsujimoto, N. Tsutsui, N. Miura, K. Kurada, H. Saka, Thin Solid Films 281–282 (1996) 562.

[8] J.C. Reiner, P. Gasser, U. Sennhauser, Microelectron. Reliab. 42 (2002) 1753.

[9] J. Loos, J.K.J. van Duren, F. Morrissey, R.A.J. Janssen, Polymer 43 (2002) 7493.

[10] D.C. Martin, J. Chen, L.F. Y.Yang, Ch. Kübel, J. Polym. Sci., B, Polym. Phys. 43 (2005) 1749.

[11] H. White, Y. Pu, M. Rafailovich, J. Sokolov, A.H. King, L.A. Giannuzzi, C. Urbanik-Shannon, B.W. Kempshall, A. Eisenberg, S.A. Schwarz, Y.M. Strzhemechny, Polymer 42 (2001) 1613.

[12] B. Schaffer, Ch. Mitterbauer, A. Schertel, A. Pogantsch, E. St. Rentenberger, F. Zojer, Ultramicroscopy 101 (2004) 123.

[13] J.M. Cairney, P.R. Munroe, Micron 34 (2003) 97.

[14] Z. Wang, T. Kato, T. Hirayama, N. Kato, K. Sasaki, H. Saka, Appl. Surf. Sci. 241 (2005) 80.

[15] J.C. Reiner, Ph. Nellen, U. Sennhauser, Microelectron. Reliab. 44 (2004) 1583.

[16] N. Virgilio, B.D. Favis, M.F. Pépin, P. Desjardins, G. L'Espérance, Macromolecules 38 (2005) 2368.

[17] H. Simmler, S. Brunner. Energy Build., in press.

[18] H. Chatham, Surf. Coat. Technol. 78 (1996) 1.

[19] M. Hanika, H.C. Langowski, U. Moosheimer, W. Peukert, Chem. Eng. Technol. 26 (2003) 605.

[20] M. Hanika, H.C. Langowski, U. Moosheimer, Proceedings of the 45th Annual Conference of the Society of Vacuum Coaters, 2002, p. 519.